X-ray Fourier transform holography by amplitude-division-type Fresnel zone plate interferometer

Minas Balyan* and Levon Haroutunyan

Faculty of Physics, Yerevan State University, Alex Manoogian 1, Yerevan 0025, Armenia.
*Correspondence e-mail: mbalyan@ysu.am

A two-block X-ray Fresnel zone plate system forms two-beams – a plane wave and a spherical wave – which interfere at the focal distance of the virtual source of the spherical wave. An object placed in the path of the plane wave forms an object wave and the spherical wave is the reference wave. The recorded intensity distribution is the Fourier transform hologram of the object. Analytical and numerical calculations show the possibilities of this scheme to record the hologram and reconstruct the object image. Examples of recording holograms of a one-dimensional cosine-like grating and a two-dimensional grid object as well as reconstruction of the images are considered.

1. Introduction

X-ray holography is one of the methods of investigating objects. In the hard X-ray region, various holographic schemes have been presented, such as X-ray in-line holography (Snigirev *et al.*, 1995; Nugent *et al.*, 1996; Paganin, 2006, and references therein), X-ray Gabor holography and Fourier transform holography (FTH) (McNulty *et al.*, 1992; Leitenberger & Snigirev, 2001; Watanabe *et al.*, 2003; Iwamoto & Yagi, 2011). Watanabe *et al.* (2004) suggested an X-ray two-zone-plates FTH scheme. X-ray dynamical diffraction holography schemes have also been presented: for example, X-ray interferometric holography (including the Momose method) (Egiazaryan & Bezirganyan, 1980; Momose, 1995; Egiazaryan, 1998; Egiazaryan *et al.*, 1998; Balyan, 2016*a,b*), X-ray Fraunhofer dynamical diffraction holography (Balyan, 2013) and X-ray Fourier transform dynamical diffraction holography (Balyan, 2015). Using hard X-ray holographic methods, the reconstruction can be performed by visible light or numerical (mathematical) methods.

Different schemes of X-ray phase contrast imaging with optical magnification based on two-block Fresnel zone plate (FZP) interferometers have been suggested (Wilhein *et al.*, 2001; Koyama *et al.*, 2004, 2006; Watanabe *et al.*, 2009). These interferometers operate in phase-front division mode. As a result, strong coherence requirements must be fulfilled. A three-plate FZP interferometer (Haroutunyan, 2015, 2016), operating in amplitude-division mode, has been suggested as well. In Fig. 1 a scheme of the interferometer is shown. The first block of the interferometer operates as a splitter, the second and third as mirror and analyzer, respectively. 'Unwanted' propagation channels arise due to the existence of multiple diffraction orders of the FZP. Suppression of the influences of those channels on the registered interference pattern is achieved by two knives located on the first and third FZPs and sufficient analyzer–image distance f. The test phase object (object from light elements) is located across the object
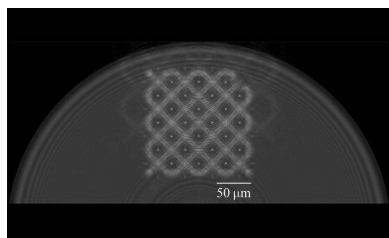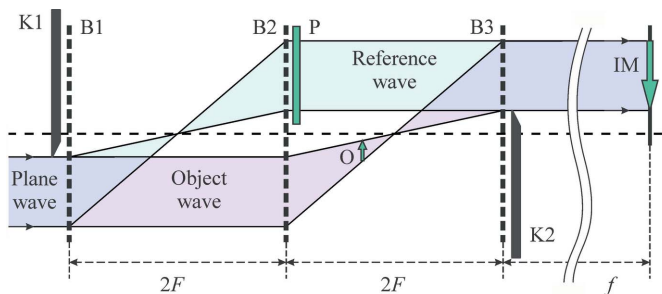
Figure 1
Experimental set-up for phase contrast imaging using a three-block FZP interferometer. B1, B2 and B3 are the blocks of the interferometer, K1 and K2 are knives, P is the phase shifter, O is the phase object and IM is phase contrast image.

wave, before it is focused in the second inter-block space, and the $\lambda/2$ phase shifter is located across the reference wave, after the second FZP (see Fig. 1). The phase contrast image is formed according to the thin lens formula.

In the present paper, based on the mentioned FZP interferometer, an X-ray FTH method is proposed and investigated both theoretically and by numerical simulation. The capabilities of the scheme for hologram recording and object image reconstruction are considered as well. In the case of a single zone plate it is known that the primary beam must be stopped (McNulty *et al.*, 1992; Leitenberger & Snigirev, 2001), which means a loss of information from the central parts of the hologram. McNulty *et al.* (1992) mentioned '*The lower spatial frequencies, corresponding to the larger scale features of the test patterns, are somewhat degraded because the beam stop blocked the central region of the hologram where the low frequencies are encoded.*' This difficulty, as also noted by Watanabe *et al.* (2004), is avoided using a two-zone-plate system. In contrast to the scheme suggested by Watanabe *et al.* (2004), the scheme considered here operates in amplitude-division mode for low-spatial-frequency structures. The corresponding hologram is recorded by low coherency requirements similar to the triple-Laue X-ray interferometer (Bonse & Hart, 1965).

As we know, for X-ray FTH schemes (see, for example, McNulty *et al.*, 1992; Leitenberger & Snigirev, 2001) where zone plates are used the detailed theory is not given. In our work the theory is given in detailed form. In particular, the necessary object–reference source distance, when the halo does not overlap with the real and conjugate images, is estimated [these estimates show that for the parameters of the scheme used by McNulty *et al.* (1992) the halo will overlap with the real and conjugate images]. In addition, in our work an expression for the reconstructed amplitude transmission coefficient has been obtained, where the background corrections are taken into account, and the quadratic phase of the specimen is also taken into account, which cannot be ignored by an object of size ~ 100 μm. The resolution is estimated based not only on the reference source size (McNulty *et al.*, 1992; Leitenberger & Snigirev, 2001) but also based on the finite size of the hologram. The maximum of these two resolutions is the real resolution in an experiment.

The coherence requirements have been estimated as well. Based on estimates of the coherency requirements it should be mentioned that X-ray synchrotron sources or X-ray free-electron lasers are needed for high-resolution imaging.

2. X-ray FZP interferometric FTH

Instead of the scheme given in Fig. 1 we consider the scheme shown in Fig. 2. The third plate of the interferometer is replaced by a photo plate or digital detector, which detects the interference intensity of the reference and object waves. The object is now placed at the same distance from the second plate as the focus point after the second plate. The wave falling onto the object may be considered as a plane wave and the wave emerging from the focus spot after the second plate may be considered as a spherical wave. Thus the detector detects the interference between the spherical wave and the wave that has passed through the object. This scheme is one of the analogues of the FTH scheme, known in optics (Hariharan, 2002). Note that in the scheme of Fig. 2 the reference wave is the object wave of Fig. 1, and *vice versa*.

Consider the conditions under which the wave propagation channels, other than the object and reference waves, do not disturb the intensity distribution of the hologram. Denote by (m, n) the channel with X-ray diffraction in m and n orders on the first and second blocks of the interferometer accordingly. Neglecting third-order and higher diffractions, nine such propagation channels will remain. Two of them, $(0,+1)$ and $(+1,+1)$, represent the reference and object waves, respectively. Consider the influence of the remaining seven channels on the registered hologram. It is easy to show in the framework of geometrical optics that six of the remaining seven 'undesirable' channels do not cross either the test object or the hologram, if the condition $d \geq R/3$ is satisfied, where d is the distance of the knife edge from the optical axes and R is the radius of the FZP (see Fig. 2). The $(+1,0)$ channel can only intersect with the upper part of the test object and the rays refracted from it at large angles can fall on the hologram. If the stronger condition $d \geq R/2$ is satisfied, the channel passes above the test object and the hologram is not distorted.

The amplitude of the wave in the detection plane is

$$E_{\mathrm{hol}} = E_{\mathrm{ref}} + E_{\mathrm{obj}}, \qquad (1)$$
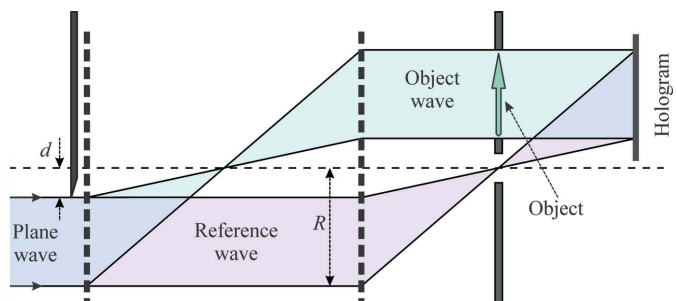
and the corresponding intensity is

Figure 2
Scheme of FTH using a two-block FZP interferometer.

$$I_{\mathrm{hol}} = |E_{\mathrm{hol}}|^2$$
$$= |E_{\mathrm{ref}}|^2 + E_{\mathrm{ref}}E_{\mathrm{obj}}^* + E_{\mathrm{ref}}^*E_{\mathrm{obj}} + |E_{\mathrm{obj}}|^2$$
$$= \sum_{i=1}^{4} I_{\mathrm{hol}\,i}. \qquad (2)$$

Here, E_{ref} is the reference wave and E_{obj} is the object wave. The detected intensity (2) is the hologram of the object under investigation.

3. Intensity distribution of the hologram and image reconstruction

Let us consider the expressions (1) and (2) analytically. A detailed scheme and coordinate systems are shown in Fig. 3. The incident wave on the object entrance surface may be considered as a plane wave with unit amplitude. Thus, the object wave in the detection plane may be written in the form

$$E_{\mathrm{obj}} = -i\frac{k}{2\pi F} \int_{-a}^{a} \int_{-a}^{a} t(X', y')$$
$$\times \exp\left\{\frac{ik}{2F}\left[(X - X')^2 + (y - y')^2\right]\right\} dX'\,dy', \quad (3)$$

where t is the amplitude transmission coefficient of the object, $2a$ is the size of the object, and the integration is performed over the exit surface of the object; k is the wavenumber. In (3) the Huygens–Fresnel principle is applied (Paganin, 2006). For the reference wave in parabolic approximation one may write

$$E_{\mathrm{ref}} \simeq \left(\frac{t_r}{r}\right)^{1/2} \exp\left[ik\left(X\sin\theta + \frac{X^2\cos^2\theta}{2\zeta_0} + \frac{y^2}{2\zeta_0}\right)\right], \quad (4)$$

where r is the intensity reflection coefficient and t_r is the intensity transmission coefficient of the FZP, ζ_0 is the distance between the focus point after the second plate and the $X = y = 0$ point of the detection plane. Since $F = \zeta_0\cos\theta$, and $\theta \approx (R + d)/2F \sim R/2F \sim 10^{-4}$ is sufficiently small, then the
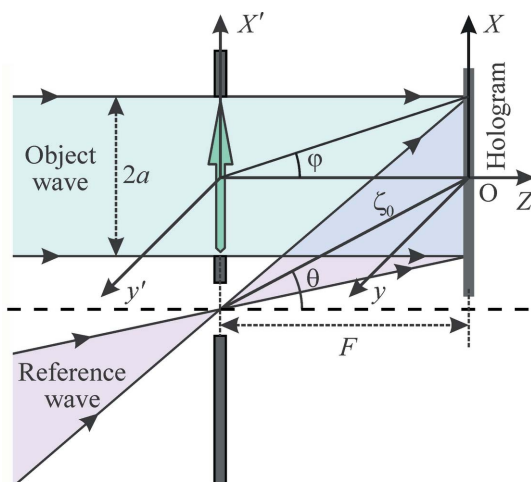

Figure 3
Coordinate system and definitions used in the FTH scheme.

approximations $\cos\theta \approx 1$, $\zeta_0 \approx F$ are valid. After these approximations, instead of equation (4) we have

$$E_{\mathrm{ref}} \simeq \left(\frac{t_r}{r}\right)^{1/2} \exp\left[ik\left(X\sin\theta + \frac{X^2}{2F} + \frac{y^2}{2F}\right)\right]. \quad (5)$$

Let us consider the third term on the right-hand side of (2),

$$I_{\mathrm{hol3}}(p, q) = -\frac{ika^2}{2\pi F}\left(\frac{t_r}{r}\right)^{1/2} \int_{-1}^{1}\int_{-1}^{1} t(aX'', ay'')$$
$$\times \exp\left[\frac{ika^2}{2F}\left(X''^2 + y''^2\right)\right] \quad (6)$$
$$\times \exp\left[-ip\left(X'' + \frac{F\sin\theta}{a}\right) - iqy''\right] dX''\,dy'',$$

where the following dimensionless coordinates are entered,

$$X_1 = X/a, \quad y_1 = y/a, \quad X'' = X'/a, \quad y'' = y'/a,$$
$$p = ka^2 X_1/F, \quad q = ka^2 y_1/F.$$

If $ka^2/F \ll 1$, the first term in the exponential under the integral sign of (6) may be neglected and (6) represents the Fourier transform of the amplitude transmission coefficient of the object. In the general case these terms must be taken into account. One may reconstruct the amplitude transmission coefficient taking the inverse Fourier transform of (6),

$$E_{\mathrm{rec3}}(u, v) = \int_{-ka^2/F}^{ka^2/F}\int_{-ka^2/F}^{ka^2/F} I_{\mathrm{hol3}}(p, q)\exp(ipu + iqv)\,dp\,dq. \quad (7)$$

Here, u and v are dimensionless parameters. The connection between them and the X and y coordinates will be established below. Integrations over p, q in the limits $(-\infty, \infty)$ give

$$E_{\mathrm{rec3}}(u, v) = -i\frac{2\pi ka^2}{F}\left(\frac{t_r}{r}\right)^{1/2} t(au - F\sin\theta, av)$$
$$\times \exp\left\{\frac{ika^2}{2F}\left[(u - F\sin\theta/a)^2 + v^2\right]\right\}. \quad (8)$$

In the same way, for the reconstruction of the second term in equation (2) we have

$$E_{\mathrm{rec2}}(u, v) = i\frac{2\pi ka^2}{F}\left(\frac{t_r}{r}\right)^{1/2} t^*(-au - F\sin\theta, -av)$$
$$\times \exp\left\{\frac{ika^2}{2F}\left[(u + F\sin\theta/a)^2 + v^2\right]\right\}. \quad (9)$$

As follows from the expression of t in equation (8), $X = au - F\sin\theta$, $y = av$. Since t is localized in the limits $-a \leq X \leq a$, $-a \leq y \leq a$, then in equation (8) the image is localized in the limits

$$\frac{F\sin\theta}{a} - 1 \leq u \leq \frac{F\sin\theta}{a} + 1, \quad -1 \leq v \leq 1, \quad (10)$$

and the conjugate image in the limits

$$-\frac{F\sin\theta}{a} - 1 \leq u \leq -\frac{F\sin\theta}{a} + 1, \quad -1 \leq v \leq 1. \quad (11)$$

The regions (10) and (11) are separated along the OX axes since $F \sin \theta > a$, which is seen from Fig. 3, where O is the origin of the coordinate system shown in Fig. 3.

For the reconstructed field of the first term in equation (2) we have

$$E_{rec1}(u, v) = \frac{t_r}{r} \int\limits_{-ka^2/F}^{ka^2/F} \int\limits_{-ka^2/F}^{ka^2/F} \exp(ipu + iqv) \, dp \, dq$$

$$= 4 \frac{t_r}{r} \frac{\sin(ka^2 u/F)}{u} \frac{\sin(ka^2 v/F)}{v}. \qquad (12)$$

Here the finite limits of integration are taken into account. As can be seen from (12), E_{rec1} along OX is localized in the region $|\Delta u| \sim \pi F/ka^2 \sim \pi/ka\theta \sim 10^{-3}$. This estimation shows that this region and images are strongly separated.

For E_{rec4} one finds

$$E_{rec4} = \frac{k^2 a^4}{F^2} \int\limits_{-1}^{1} \int\limits_{-1}^{1} t(aX', ay') t^*\left[a(X' - u), a(y' - v)\right] \qquad (13)$$

$$\times \exp\left\{\frac{ika^2}{2F}\left[X'^2 - (X' - u)^2 + y'^2 - (y' - v)^2\right]\right\}$$

$$\times dX' \, dy',$$

if

$$u \in [-2, 2], \qquad (14)$$

and $E_{rec4} = 0$ otherwise. Thus, E_{rec4} forms a halo around the centre of the reconstructed field. As can be seen from (10), (11) and (14), the halo does not intersect with the images when $a \leq F \sin \theta/3$, which is equivalent to the condition

$$d \geq R/2, \qquad (15)$$

since $a = (R - d)/2$ and $F \sin \theta \simeq F\theta = a + d$. It should be mentioned that the condition (15) must be strongly satisfied when the amplitude transmission coefficient is determined, but it may not be strongly satisfied if an object image is reconstructed.

4. Determination of the amplitude transmission coefficient

The reconstructed field may be written as

$$E_{rec} = E_{rec1} + E_{rec2} + E_{rec3} + E_{rec4}. \qquad (16)$$

If the condition (15) is fulfilled, in the region of the image $E_{rec}(u, v) \approx E_{rec3}(u, v)$. Using the hologram, one may calculate $E_{rec}(u, v)$ and, in the region of the image,

$$t(au - F \sin \theta, av) = i\frac{F}{2\pi ka^2}\left(\frac{r}{t_r}\right)^{1/2}$$

$$\times \exp\left\{-\frac{ika^2}{2F}\left[(u - F \sin \theta/a)^2 + v^2\right]\right\}$$

$$\times E_{rec3}(u, v)$$

$$\simeq i\frac{F}{2\pi ka^2}\left(\frac{r}{t_r}\right)^{1/2} \qquad (17)$$

$$\times \exp\left\{-\frac{ika^2}{2F}\left[(u - F \sin \theta/a)^2 + v^2\right]\right\}$$

$$\times E_{rec}(u, v).$$

For each value of (u, v) taken in the region (10) the corresponding coordinates of the object can be found as $X = au - F \sin \theta$, $y = av$, and for these values using the known $E_{rec}(u, v)$ the amplitude transmission coefficient $t(X, y)$ may be found according to (17).

5. Resolution

The resolution of the scheme is determined by three factors: the size of the reference source, the finite sizes of the hologram and the resolution of the detector (McNulty *et al.*, 1992; Leitenberger & Snigirev, 2001). As has been mentioned by Leitenberger & Snigirev (2001), '*a hologram recording using a lower resolution detector does not change the achievable image resolution*'. The fact that the resolution in FTH is independent of the resolution of the detector has been mentioned by Watanabe *et al.* (2004) as well. This fact is also known in optics (Stroke *et al.*, 1965). So the maximum of the reference source size and the resolution determined by the finite sizes of the hologram is the resolution of the scheme. The size of the reference source is the size of the focus spot of the FZP, which is equal to the size of the outermost Fresnel zone. This type of resolution has been considered in detail (McNulty *et al.*, 1992; Leitenberger & Snigirev, 2001).

Consider the resolution, determined by the finite sizes of the hologram. The object may have a continuous distribution of matter or may consist of localized points. Let us first determine the resolution of the scheme for the case of a continuous amplitude transmission coefficient. Let us turn to the formulae of the reconstruction (6)–(9). The integrations over p, q, if one takes the limits $(-\infty, \infty)$, give the δ-functions

$$\int\limits_{-\infty}^{\infty} \int\limits_{-\infty}^{\infty} \exp\left[-ip\left(X'' + \frac{F \sin \theta}{a} - u\right) - iq(y'' - v)\right] dp \, dq$$

$$= (2\pi)^2 \delta\left(X'' + \frac{F \sin \theta}{a} - u\right)\delta(y'' - v). \qquad (18)$$

For finite size holograms in the formulas of reconstruction (6)–(9) we must take into account the finite integration limits when integrating over (p, q). As a result, instead of δ-functions one finds

$$\int\limits_{-ka^2/F}^{ka^2/F} \int\limits_{-ka^2/F}^{ka^2/F} \exp\left[-ip\left(X'' + \frac{F\sin\theta}{a} - u\right) - iq(y'' - v)\right] dp\, dq$$

$$= \frac{2\sin\frac{ka^2}{F}\left(X'' + \frac{F\sin\theta}{a} - u\right)}{\left(X'' + \frac{F\sin\theta}{a} - u\right)} \frac{2\sin\frac{ka^2}{F}(y'' - v)}{(y'' - v)}. \qquad (19)$$

In dimensional coordinates this gives the effective integration region about $2\pi F/ka$. In dimensional coordinates the function $t(X, y)$ around the central point $(X_0, y_0) = (au - F\sin\theta, av)$ of equation (19) may be approximated as $t(X, y) = t(X_0, y_0) + t_X(X_0, y_0)\Delta X + t_y(X_0, y_0)\Delta y$. For resolving the object the variation $t(X, y) - t(X_0, y_0) = t_X(X_0, y_0)\Delta X + t_y(X_0, y_0)\Delta y$ of the amplitude transmission coefficient when $|\Delta X| = |\Delta y| = \pi F/ka$ must be less than the average value of the modulus of t, i.e. $|t_X(X_0, y_0)|\pi F/ka \ll |\bar{t}|$, $|t_y(X_0, y_0)|\pi F/ka \ll |\bar{t}|$. This means that continuous amplitude transmission coefficients may be reconstructed which are almost constant in the regions with size $\pi F/ka$ in both directions X and y.

If the object contains localized inhomogeneities, two inhomogeneities (points) that are separated by the distances $\pi F/ka$ in both X and y directions may be resolved.

So, the resolution determined by the finite sizes of the hologram for both directions in dimensional coordinates is about

$$\pi F/ka = R^2/2aN = 4R/2N = 4\Delta R_N, \qquad (20)$$

where $\Delta R_N = R/2N$ is the size of the outermost zone. In (20), for definiteness, $d = R/2$ ($a = R/4$) is taken.

6. Coherency requirements

The spatial and temporal coherency requirements of the incident radiation are determined by the scattering angle of the object wave on the object. The trajectories of the object and reference wave for both small and large scattering angles are shown in Fig. 4. As can be seen from Fig. 4, for small scattering angles the interferometer operates in amplitude-division mode with an equal path of trajectories in both channels of propagation. As a result the scheme works under low spatial and temporal coherency requirements of incident
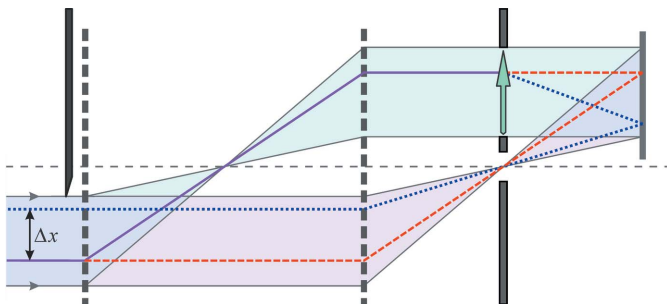

Figure 4
Trajectories of object and reference waves interfering at the same point of the hologram. A ray of the object wave falling on the object is indicated by the solid line, and that scattered on the object at low angles and the reference wave rays are indicated by dashed lines. The dotted lines indicate the rays related to the case of large angle scattering.

radiation. For large scattering angles the interferometer does not work in amplitude-division mode. The trajectories of the rays, coming to the same point of the hologram, are separated on the entrance surface of the interferometer. The maximal separation in the transverse direction is $\Delta x_m = \Delta y_m = 2a$, and maximal path difference is $\Delta l_m \simeq 2R(R - d)/F$. The longitudinal (temporal) coherence length l_L is connected to the quasimonochromaticity of the beam, $l_L = \lambda^2/\Delta\lambda$. Here, $\Delta\lambda$ is the range of wavelengths in the incident beam. The quasimonochromaticity does not disturb the intensity distribution of the hologram when the requirement $l_L \geq \Delta l_m$ is satisfied. According to the Van Cittert–Zernike theorem (Born & Wolf, 2002) the spatial (transverse) coherence length $l_T = L\lambda/u_s$, where u_s is the size of the source and L is the source-to-system distance. l_T is connected to the size of the source. The size of the source does not disturb the intensity distribution of the hologram, when the condition $l_T \geq 2a$ is fulfilled. In particular, taking $d = R/2$ [see equation (15)], one obtains the following conditions of coherency: $l_L \geq R^2/F = \lambda N$ and $l_T \geq R/2$, where N is the number of zones.

Large-scale features of the object under investigation correspond to low spatial Fourier harmonics and low scattering angles of the object wave. In this case the hologram may be recorded under low coherency requirements. Small-scale features of the object correspond to high spatial Fourier harmonics and large scattering angles of the object wave. Accordingly the coherency requirements increase up to l_L for temporal and l_T for spatial coherences.

7. Examples

Consider two examples of hologram recording and reconstruction.

Example (1). Consider the amplitude transmission coefficient $t(X)$ of a one-dimensional cosine grating, which is given by the expression

$$t(X) = \cos^2 \pi X/\Lambda, \qquad (21)$$

where $\Lambda = 4\,\mu m$ is taken. The case where the radiation wavelength $\lambda = 0.1\,nm$, FZP focal length $F = 1\,m$, FZP radius $R = 195\,\mu m$, outermost Fresnel zone size $= 0.25\,\mu m$, $a = 0.25R$ ($d = R/2$), $\theta = 1.46 \times 10^{-4}$ and $F\sin\theta = 0.75R$ is considered. The resolution due to the finite size of the reference source is $0.25\,\mu m$ and according to (20) the resolution determined by the finite size of the hologram is $1\,\mu m$. The resulting resolution will be $1\,\mu m$. The image and conjugate image are located in the limits $2 \leq u \leq 4$ and $-4 \leq u \leq -2$, respectively; the halo and primary reconstructed field are located in the limits $-2 \leq u \leq 2$. In Fig. 5 the corresponding hologram intensity distribution is presented. The calculations are made using equation (2) taking into account the finite limits of the hologram. In Fig. 6 the real and imaginary parts of the reconstructed amplitude transmission coefficient are shown. The reconstructed image is disturbed by the background, formed due to the reconstructed reference wave amplitude. This background is sufficiently high, since the amplitude of the reference wave is more than two times larger compared with
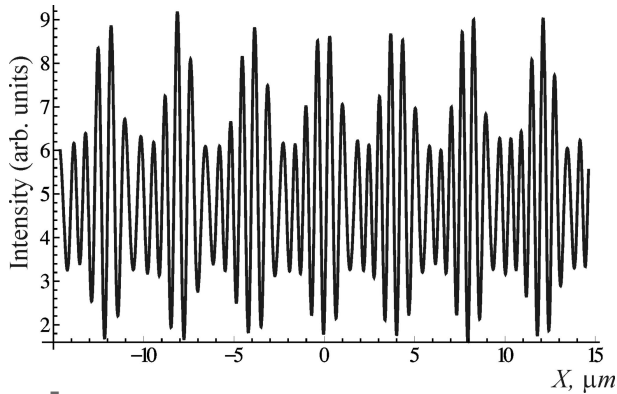
Figure 5
Two-block FZP FTH hologram of a one-dimensional cosine grating.

the amplitude of the object wave. This background may be taken into account using the formulae (12) and (17). Formula (17) may be rewritten as

$$t(au - F\sin\theta, av) \simeq i\frac{F}{2\pi ka^2}\left(\frac{r}{t_r}\right)^{1/2}$$

$$\times \exp\left\{-\frac{ika^2}{2F}\left[(u - F\sin\theta/a)^2 + v^2\right]\right\}$$

$$\times \left[E_{rec}(u, v) - E_{rec1}(u, v)\right]. \qquad (22)$$

The reconstructed amplitude transmission coefficient, taking into account the background correction, is shown in Fig. 7. It can be seen that in the middle part of the reconstructed image
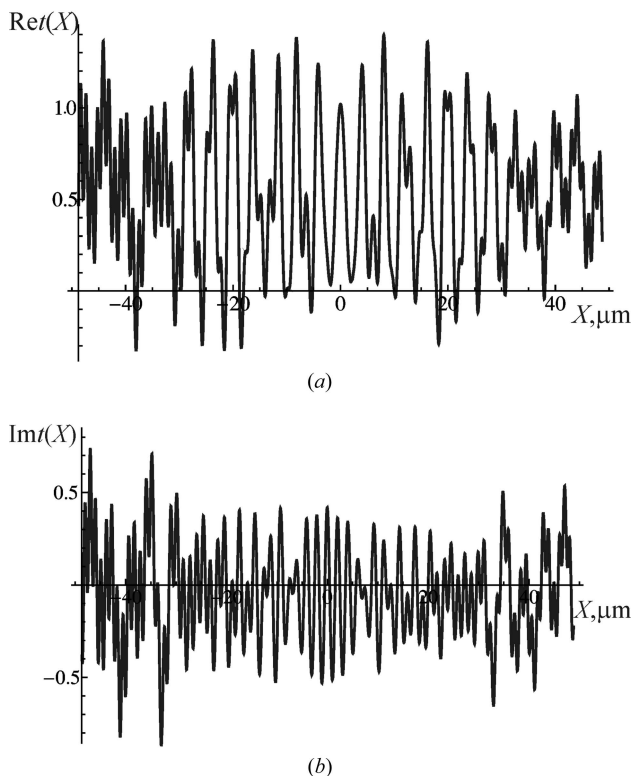
the reconstructed values are close to the values of the object amplitude transmission coefficient. At the edges the resolution is low. $E_{rec}(u, v)$ is calculated using (16), in which for the first three terms the finite size of the hologram is taken into account, and for the fourth term the formula (13) is used for simplicity.

Example (2). The numerical simulation of the hologram of the two-dimensional amplitude object (see Fig. 8), as well as further image reconstruction, was performed (Fig. 9). The following values of the main experimental parameters were used in the numerical calculations: $\lambda = 0.1$ nm, $F = 1$ m, $R = 275.7$ µm, FZP outermost zone width = 181.5 nm, $d = 43.1$ µm, half-width of rectangle test object $a = 78.6$ µm. As can be seen from a comparison of Figs. 8(a) and 9, the reconstructed image matches well with the tested object. The authors consider that the noise at the bottom of the reconstructed image, as well as the radial pattern in its lower half, are caused by the failure of above-mentioned condition $d \geq R/3$, required for blocking of 'unwanted' channels of the wave propagation. As a result, part of the propagation channel (+1,0), passing through the test object, falls on the hologram. The additional numerical simulations, performed for different values of d, show the vanishing of the mentioned imperfections of reconstruction at $d = R/3$ and higher. The value of d in the case of Fig. 9 was chosen as $d = 0.156R$, with the aim to increase the size of the tested object as much as possible.
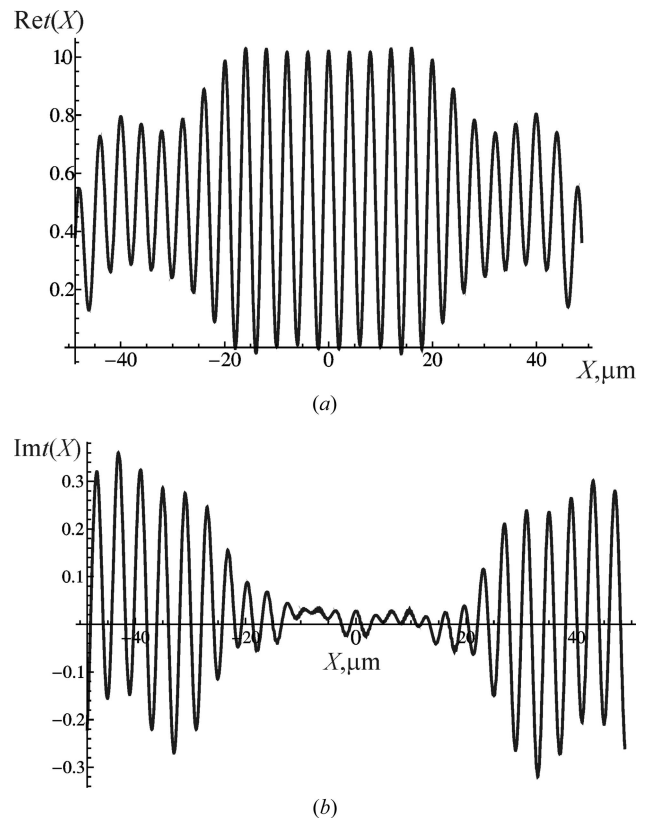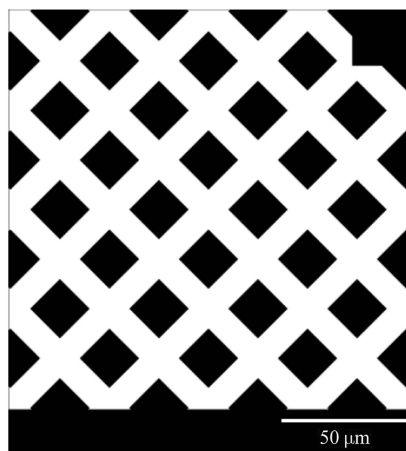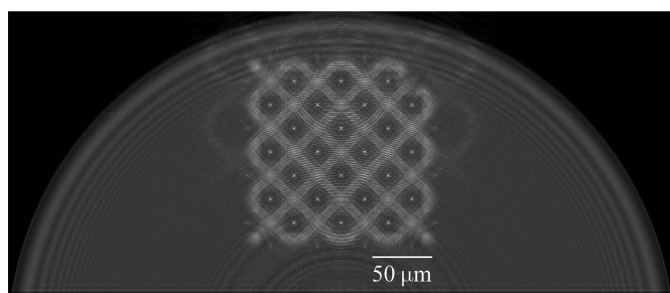

(*a*)

(*b*)

Figure 6
(*a*) Real and (*b*) imaginary parts of the reconstructed amplitude transmission coefficient of the cosine grating without background correction.

(*a*)

(*b*)

Figure 7
(*a*) Real and (*b*) imaginary parts of the reconstructed amplitude transmission coefficient of the cosine grating taking into account background correction.

(a)

(b)

Figure 8
(a) Two-dimensional amplitude object and (b) numerically simulated hologram.

Figure 9
Reconstructed two-dimensional object image from the simulated hologram.

8. Summary

In this paper an X-ray FTH scheme based on a two-block FZP interferometric system operating in amplitude-division mode is suggested and theoretically and numerically considered. In the case of recording the low-spatial-frequency structures of the object the interferometer operates in amplitude-division mode and does not impose high requirements on the coherency of the initial radiation. The capability of the scheme to reconstruct the amplitude transmission coefficient of the amplitude and phase objects is shown. The resolution and coherence requirements of the scheme are estimated. Examples of reconstruction of the amplitude transmission coefficient of a cosine grating and a two-dimensional object image are considered. This scheme may be part of an X-ray microscope, and may be realised using both synchrotron sources of X-ray radiation and X-ray free-electron lasers.

References

Balyan, M. (2013). *J. Synchrotron Rad.* **20**, 749–755.
Balyan, M. (2015). *J. Contemp. Phys.* **50**, 394–403.
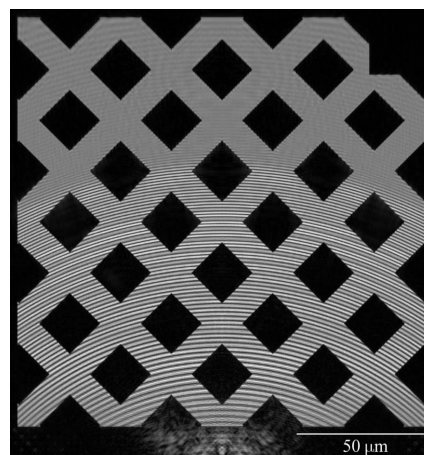Balyan, M. (2016a). *J. Contemp. Phys.* **51**, 79–88.
Balyan, M. (2016b). *J. Contemp. Phys.* **51**, 289–298.
Bonse, U. & Hart, M. (1965). *Appl. Phys. Lett.* **6**, 155–156.
Born, M. & Wolf, E. (2002). *Principles of Optics*, 7th ed. Cambridge University Press.
Egiazaryan, A. M. (1998). *Pisma Zh. Tech. Fiz.* **24**, 55–59.
Egiazaryan, A. M. & Bezirganyan, P. A. (1980). *Proc. Nat. Acad. Sci. Armen. Phys.* **15**, 35–43.
Egiazaryan, A. M., Trouni, K. G. & Mkrtchyan, A. R. (1998). *Pisma Zh. Exp. Teor. Fiz.* **68**, 681–684.
Hariharan, P. (2002). *Basics of Holography*. Cambridge University Press.
Haroutunyan, L. A. (2015). *J. Contemp. Phys.* **50**, 292–295.
Haroutunyan, L. A. (2016). *J. Contemp. Phys.* **51**, 284–288.
Iwamoto, H. & Yagi, N. (2011). *J. Synchrotron Rad.* **18**, 564–568.
Koyama, T., Kagoshima, Y., Wada, I., Saikubo, A., Shimose, K., Hayashi, K., Tsusaka, Y. & Matsui, J. (2004). *Jpn. J. Appl. Phys.* **43**, L421–L423.
Koyama, T., Tsuji, T., Yoshida, K., Takano, H., Tsusaka, Y. & Kagoshima, Y. (2006). *Jpn. J. Appl. Phys.* **45**, L1159–L1161.
Leitenberger, W. & Snigirev, A. J. (2001). *J. Appl. Phys.* **90**, 538–544.
McNulty, I., Kirz, J., Jacobsen, C., Anderson, E. H., Howells, M. R. & Kern, D. P. (1992). *Science*, **256**, 1009–1012.
Momose, A. (1995). *Nucl. Instrum. Methods Phys. Res. A*, **352**, 622–628.
Nugent, K. A., Gureyev, T. E., Cookson, D. F., Paganin, D. & Barnea, Z. (1996). *Phys. Rev. Lett.* **77**, 2961–2964.
Paganin, D. M. (2006). *Coherent X-ray Optics*. Oxford University Press.
Snigirev, A., Snigireva, I., Kohn, V., Kuznetsov, S. & Schelokov, I. (1995). *Rev. Sci. Instrum.* **66**, 5486–5492.
Stroke, G. W., Brumm, D. & Funkhouser, A. (1965). *J. Opt. Soc. Am.* **55**, 1327–1328.
Watanabe, N., Hoshino, M., Yamamoto, K., Aoki, S., Takeuchi, A. & Suzuki, Y. (2009). *J. Phys. Conf. Ser.* **186**, 012021.
Watanabe, N., Yokosuka, H., Ohogashi, T., Takano, H., Takeuchi, A., Suzuki, Y. & Aoki, S. J. (2003). *J. Phys. IV Fr.* **104**, 551–556.
Watanabe, N., Yokosuka, H., Ohogashi, T., Takano, H., Takeuchi, A., Suzuki, Y. & Aoki, S. J. (2004). *AIP Conf. Proc.* **705**, 1340–1343.
Wilhein, T., Kaulich, B. & Susini, J. (2001). *Opt. Commun.* **193**, 19–26.